RSC Advances

ROYAL SOCIETY OF CHEMISTRY

www.rsc.org/advances

Journal Name

RSCPublishing

Size-selected boron nitride nanosheets as oxygen-atom corrosion resistant fillers

Cite this: DOI: 10.1039/x0xx00000x

Min Yi,*[ab] Zhigang Shen,*[a] Lei Liu,[a] and Shuaishuai Liang[a]

Received ooth January 2012,
Accepted ooth January 2012

DOI: 10.1039/x0xx00000x

www.rsc.org/

Size-selected boron nitride nanosheets (BNNSs) were explored to enhance the polymer's oxygen-atom corrosion resistance. BNNSs with three kinds of average lateral size were prepared by a size selection route. All these BNNSs could enhance the polymer's oxygen-atom corrosion resistance, but we found much greater enhancement by using larger BNNSs, i.e. adding ~1.0 wt% large BNNSs (~21.4 μm^2) can achieve 87% decrease in the polymer' mass loss. BNNSs' barrier and bonding effects are responsible for the enhanced resistance. These results throw light on resisting oxygen-atom corrosion by BNNSs with controllable size.

Two-dimensional boron nitride nanosheets (BNNSs) have been widely investigated in both fundamental and application aspects. BNNSs show better performance than the bulk counterpart in such fields as transistors, solid lubricant, thermal conductors, etc.[1-3] Apart from these metrics, BNNSs have some special physical and chemical properties. For example, like graphene which shows impermeability to standard gas,[4] BNNS possesses excellent barrier properties.[5, 6] BNNS also has excellent thermal stability and remarkable inertness to oxidizing gas and liquid solutions.[7] Furthermore, BNNS is hydrophobic by nature and it can passivate surfaces effectively from water.[8] These exceptional properties make BNNS uniquely suitable as an anticorrosion material. The investigation of oxidation resistance of BNNS is important for its application.

Initially, BN coatings were directly grown on substrates and improved the high-temperature oxidation resistance of the substrate material.[9, 10] Most recently, Husain et al. incorporated BN particles into polymers to form composite coatings, which showed improved resistance to electrochemical corrosion.[11] Liu et al. reported the use of ultrathin grown BN as high-performance oxidation-resistant coatings for nickel up to 1,100 °C in oxidizing atmospheres.[12] Li et al. reveal that monolayer BN nanosheets can sustain up to 850 °C based on the BNNS prepared by micromechanical cleavage.[13] Yi et al. reported the application of BNNSs in resisting oxygen-atom corrosion.[14-16] To extend these works, the study and application of BNNSs in corrosion fields are highly recommended to go further.

Herein, we focus on the oxygen-atom corrosion resistance of polymer by adding BNNSs with controllable size. In oxygen atom, two unpaired electrons gives ^{3}p oxygen two reactive sites. The highly oxidative oxygen atom can result in heavy and quick corrosion of polymer surface. Even in the dry or vacuum environment, for example in the low earth orbit (LEO), a very small amount of oxygen atom can easily corrode the polymer heavily. One potential application of this topic is enhancing the oxygen-atom corrosion resistance of the spacecraft polymeric parts in LEO where oxygen atom exists; because corrosion induced by space environment has huge danger.

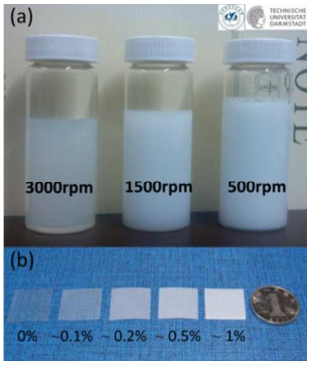

Fig. 1 (a) Photographs of PVA/BNNSs composite dispersions obtained by a centrifugation based size selection route. (b) Photographs of PVA/BNNSs composite films with different loading of large BNNSs.

Polyvinylalcohol (PVA) was chosen as a model polymer to form composites with BNNSs. In order to prepare composites, we firstly prepared PVA/BNNSs dispersions by sonication and centrifugation (see ESI† for detail). With PVA as stabilizer, BNNSs can be stabilized in water to form homogeneous

colloid, as shown in Fig. 1a. We adopted controlled centrifugation to select BNNSs with different lateral size.[17-19] The concentration was estimated from the BNNSs content, which was roughly measured by the TGA (thermal gravimetric analysis) curves of the dried PVA/BNNSs composites (see ESI†). Firstly, a centrifugation speed of 3000rpm (revolutions per minute), corresponding to a centrifugal acceleration of 2304g was used to obtain ~0.22 mg/mL BNNSs dispersions which should contain small BNNSs. Then we collected the sediment and diluted it by PVA solution. The diluted dispersions were further bath sonicated and centrifuged at a low rotation speed of 1500rpm (×576g). The resultant dispersions contain medium BNNSs, with a concentration of ~0.94 mg/mL. Repeating this route at 500rpm (×64g) can achieve ~2.8 mg/mL dispersions which should contain large BNNSs.

A typical atomic force microscopy (AFM) image of the small BNNSs is shown in Fig. 2. The bright spots in the AFM image are the residual PVA after water evaporation. Because of the residual PVA, it is very difficult to obtain high-quality AFM images and AFM tips are often damaged. More AFM images of these three kinds of BNNSs are shown in Fig. 3. It can be seen that all the large, medium, and small BNNSs have a thickness less than 3.0 nm. This thickness size confirms the high degree of exfoliation and thus the BNNSs' high quality. These several atomic-layered flakes also ensure the large aspect ratio which has been deemed as an important parameter in reinforcing composites. Through statistical analysis of AFM images, the lateral size of the BNNSs is quantitatively estimated. The small BNNSs before size selection have an average area (<A>) of ~1.0 μm^2. The medium and large BNNSs achieved by size selection are of much larger area, with <A> ~4.1 μm^2 and <A> ~21.4 μm^2, respectively. This statistical analysis confirms the effectiveness of selecting BNNSs lateral size by controlled centrifugation.

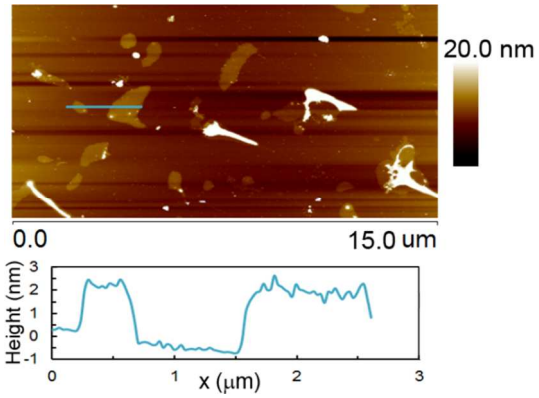

Fig. 2 A typical AFM image of small BNNSs and the height profile.

Free standing composite films were prepared by solution casting of these PVA/BNNSs composite dispersions (see ESI† for details). The enhancement in thermal stability also indicates strong interactions between the BNNS fillers and PVA matrix (Fig. S1 in ESI†). Oxygen-atom exposure was carried out in a ground-based atom oxygen effect simulation facility (see ESI† for details).[19-21] The samples are cut into 10 mm×10 mm, as shown the photographs in Fig. 1b.

Shown in Fig. 4 are the scanning electron microscopy (SEM) images of the oxygen-atom corroded surface of pure PVA and composite films. Apparently, the surface morphology after oxygen-atom exposure is greatly distinct. The pure PVA film

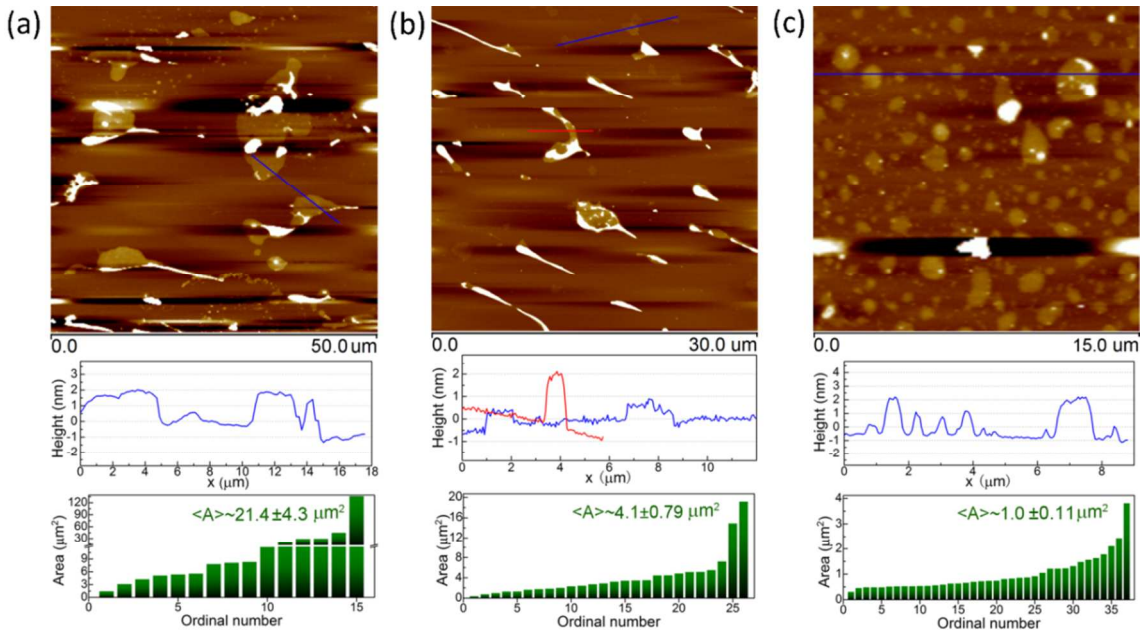

Fig. 3 Typical AFM images, height profiles, and BNNSs' area distribution of (a) large BNNSs after centrifugation of 500rpm, (b) medium BNNSs after centrifugation of 1500rpm, and (c) small BNNSs after centrifugation of 3000rpm. The bright spots in AFM images are the residual PVA after water evaporation.

surface is severely corroded and roughened, exhibiting "carpet-like" structures with deep caves (Fig. 4a). As shown in Fig. 4b-d, the surface morphology is totally different among the composite films filled with BNNSs of different size. In the composite film with small BNNSs (Fig. 4b), "carpet-like" structures also appear, but the caves are slightly relieved. In the inset of Fig. 4b, lots of tiny BNNSs can be seen. In the case of large BNNSs, "carpet-like" structures are negligible at a large-BNNSs loading of ~0.5 wt%, as shown in Fig. 4c. The size of the exposed BNNSs seems consistent with the average area estimated by AFM in Fig. 3. Most interestingly, when the loading reaches ~1.0 wt%, the exposed surface is readily covered with BNNSs. It can be anticipated that if the corroded surface is well covered by BNNSs, the corrosion resistance will be high. In contrast, if the surface is dominated by "carpet-like" morphologies, a low corrosion resistance will be achieved.

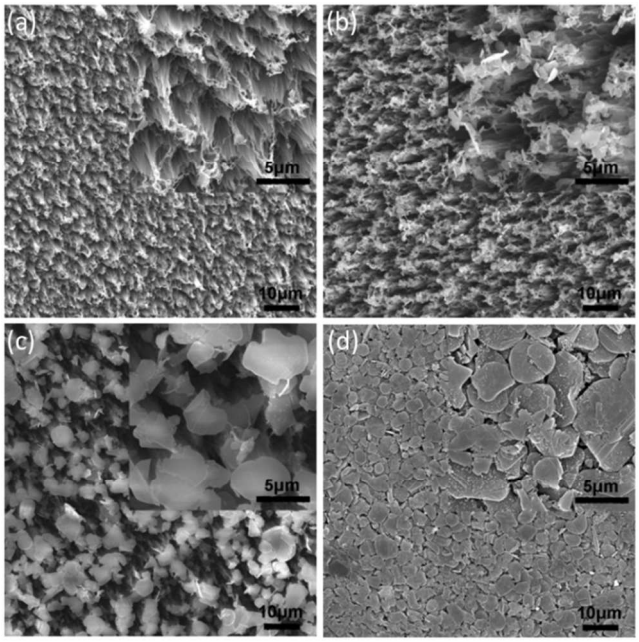

Fig. 4 Surface SEM images of (a) pure PVA film, (b) ~0.7 wt% small-BNNSs/PVA film, (c) ~0.5 wt% and (d) ~1.0 wt% large-BNNSs/PVA film after exposed oxygen atom.

X-Ray photoelectron spectrometer (XPS) was used to analyse the composition of the corroded surface, as shown in Fig. 5. Form the B1s and N1s spectra in Fig. 5a, it can be seen that no oxidation is induced during the BNNSs preparation. As shown in Fig. 5b, in the surface of pure PVA, the content of oxygen remarkably increases after the oxygen-atom exposure. This indicates the reaction of oxygen atom with PVA. For PVA/BNNSs film, the exposed surface has the component of B and N, as shown in Fig. 5c. This implies that PVA is corroded away while BNNSs remain, in accordance with the SEM results in Fig. 4. As shown in Fig. 5d, N1s spectrum keeps a single peak, while B1s spectrum becomes asymmetric with a fitted peak associated with B-O bond. This indicates that BNNSs have reacted with oxygen atom, and it is B rather than N that reacts with oxygen atom.

The mass loss has also been the critical parameter for quantitatively valuing the oxygen-atom corrosion resistance of a material. We have plotted the mass loss as a function of the fillers' loading, as shown in Fig. 6. In the oxygen-atom corrosion case, because the corrosion products are often volatilizable gas, the mass increase by oxygen atom can be neglectful. Obviously, after filling BNNSs, the mass loss of PVA decreases. At the same loading, larger BNNSs' size leads to more notable enhancement in oxygen-atom resistance. As shown in Fig. 6, an addition of ~0.2 wt% large BNNSs, ~0.22 wt% medium BNNSs, and ~0.28 wt% small BNNSs can achieve ~49, ~42, and 27% decreases in mass loss, respectively. Only ~1.0 wt% large BNNSs could result in a mass loss reduction of ~87%. For the case of large BNNSs, a saturation appears at high loading content of BNNSs. For comparison, we have also added pristine BN powder to reinforce PVA, but to find that 1.5 wt% BN powder could only result in ~42% decrease in mass loss, even lower than that in the case of ~0.2 wt% large-BNNSs loading. Therefore, the reduction in mass loss indicates that BNNSs fillers can improve the oxygen-atom corrosion resistance of polymer. These results are very attractive when compared to that by adding traditional fillers. For example, ~5 wt% nano SiO_2 can only lead to a reduction of ~42% in mass loss.[22] An extremely high loading of plerospheres (~50 wt%) can only lead to a reduction of ~68% in

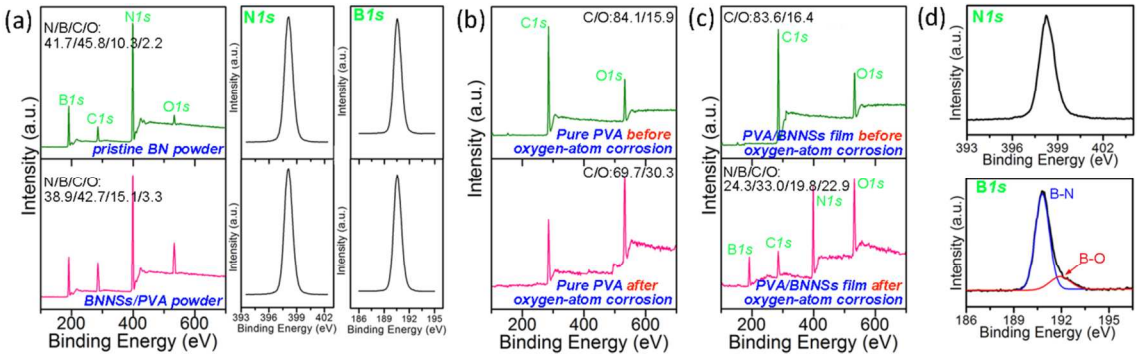

Fig. 5 (a) XPS results of pristine BN powder and BNNSs/PVA powder. XPS survey of the surfaces of (b) pure PVA and (c) ~0.5 wt% large-BNNSs/PVA film before and after oxygen-atom exposure. (d) N1s and B1s spectra in (c) after oxygen-atom exposure.

mass loss[23]. When compared to the work on graphene and graphene oxide in which 1 wt% large graphene can only achieve 42% decrease in composites' mass loss,[19] BNNSs also show much better performance in resisting oxygen-atom corrosion. In this aspect, it has significant advantages that BNNSs fillers with these low loadings can match the performance of large quantities of traditional fillers in improving oxygen-atom corrosion resistance.

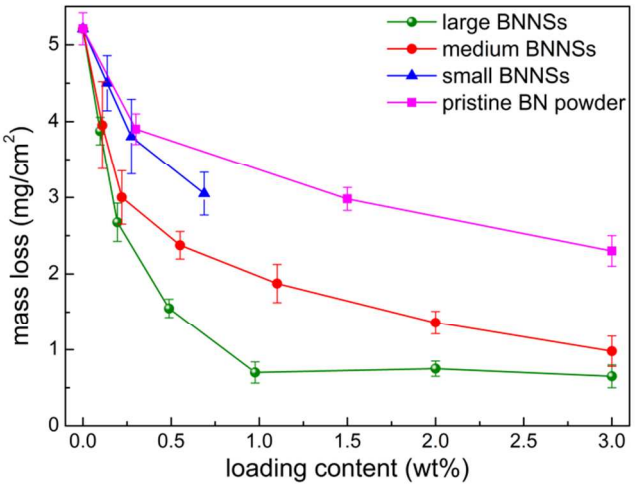

Fig. 6 Mass loss of PVA/BNNSs films with different loading of large BNNSs, medium BNNSs, small BNNSs, and pristine BN powder after exposed into oxygen atom.

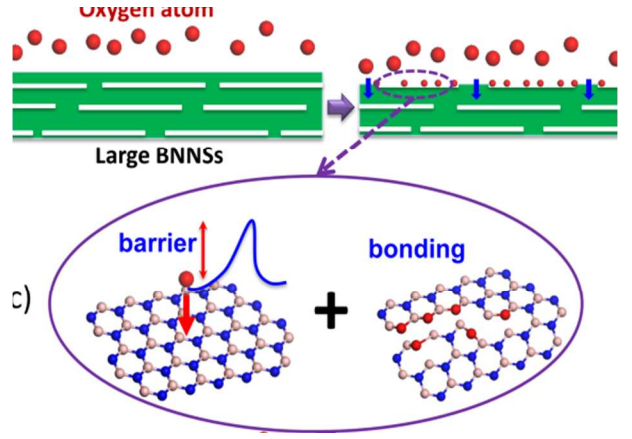

Fig. 7 Schematic of the mechanism that BNNSs can enhance oxygen-atom corrosion resistance of PVA composites. (a) Large BNNSs allow less penetrative channels. (b) Small BNNSs allow more penetrative channels. (c) Two possible routes for the mechanism.

We suggest that two effects contribute to the anticorrosion mechanism of BNNSs in resisting oxygen-atom corrosion, as shown in Fig. 7. The first is barrier effect. Because BN layers are revealed to have barrier effects for oxygen-atom penetration and protect polymer underneath from corrosion. However, BNNSs with different size have different performance. Larger BNNSs have much fewer edges and allow much less penetrative channels than smaller ones, resulting in much better barrier effect, as illustrated in Fig. 7a and b. The second is bonding effect. Recent experimental study has shown that oxygen atom induced oxidation of monolayer BN occurs through a gradual substitution of N by O in the h-BN lattice,[24] and an efficient oxygen-healing mechanism exists in BN structure with N vacancies.[25] Though B is oxidized by O, N is removed. Hence, the oxygen atom induced increase in the mass of BN can also be neglectful. It can be anticipated that these flaked BNNSs with large surface area are inclined to react with atom oxygen to form bonds. This can resist subsequent corrosion and alleviate PVA matrix corrosion by consuming abundant oxygen atom. The bonding mechanism can be verified by the B-O peak in Fig. 5d.

In conclusion, the potential of BNNSs as fillers to enhance the oxygen-atom corrosion of polymeric composites has been explored. By sonication and centrifugation-based size selection, we prepared BNNSs/PVA hybrid dispersions with BNNSs of three different averaged area, large: ~21.4 μm^2, medium: ~3.1 μm^2, and small: ~1.0 μm^2. Results from SEM, XPS, and mass loss prove that all these BNNSs fillers can enhance oxygen-atom corrosion resistance. Large BNNSs perform much better than the smaller ones. Adding only ~1.0 wt% large BNNSs can achieve 87% decrease in composites' mass loss. BNNSs' bonding and barrier effects could be responsible for the enhanced resistance. Large-surface-area BNNSs can react with oxygen atom to form bonds, thus consuming abundant oxygen atom. Larger BNNSs have much better barrier effects and thus much higher resistance. We hope that these preliminary results could establish BNNSs as the novel fillers for resisting oxygen-atom corrosion.

Acknowledgements

The authors acknowledge financial support by the Beijing Natural Science Foundation (2132025), Specialized Research Fund for the Doctoral Program of Higher Education (20131102110016), the Innovation Foundation of BUAA for Ph.D. Graduates (YWF-14-YJSY-052), and the China Scholarship Council (CSC).

Notes and references

[a] *Beijing Key Laboratory for Powder Technology Research and Development, Beijing University of Aeronautics and Astronautics, Beijing 100191, China.*
[b] *Institute of Materials Science, Technische Universität Darmstadt, Darmstadt 64287, Germany.*

Fax:+ 86 10-82338794; Tel: +86 10-82317516;
E-mail: yimin@buaa.edu.cn; shenzhg@buaa.edu.cn

† Electronic Supplementary Information (ESI) available: experimental details and additional data. See DOI: xx.xxxx/b000000x/

1. D. Golberg, Y. Bando, Y. Huang, T. Terao, M. Mitome, C. Tang and C. Zhi, *ACS Nano*, 2010, **4**, 2979-2993.
2. Y. Lin and J. W. Connell, *Nanoscale*, 2012, **4**, 6908-6939.

3. M. Xu, T. Liang, M. Shi and H. Chen, *Chem. Rev.*, 2013, **113**, 3766-3798.
4. J. S. Bunch, S. S. Verbridge, J. S. Alden, A. M. van der Zande, J. M. Parpia, H. G. Craighead and P. L. McEuen, *Nano Lett.*, 2008, **8**, 2458-2462.
5. H. Cun, M. Iannuzzi, A. Hemmi, S. Roth, J. Osterwalder and T. Greber, *Nano Lett.*, 2013, **13**, 2098-2103.
6. A. Itakura, M. Tosa, S. Ikeda and K. Yoshihara, *Vacuum*, 1996, **47**, 697-700.
7. C. C. Tang, Y. Bando, T. Sato, K. Kurashima, X. X. Ding, Z. W. Gan and S. R. Qi, *Appl. Phys. Lett.*, 2002, **80**, 4641.
8. A. Pakdel, C. Zhi, Y. Bando, T. Nakayama and D. Golberg, *ACS Nano*, 2011, **5**, 6507-6515.
9. A. Nechepurenko and S. Samuni, *J. Solid State Chem.*, 2000, **154**, 162-164.
10. C. Tang and Y. Bando, *Appl. Phys. Lett.*, 2003, **83**, 659.
11. E. Husain, T. N. Narayanan, J. J. Taha-Tijerina, S. Vinod, R. Vajtai and P. M. Ajayan, *Acs Appl. Mater. Interfaces*, 2013, **5**, 4129-4135.
12. Z. Liu, Y. Gong, W. Zhou, L. Ma, J. Yu, J. C. Idrobo, J. Jung, A. H. Macdonald, R. Vajtai, J. Lou and P. M. Ajayan, *Nat. Commun.*, 2013, **4**, 2541.
13. L. H. Li, J. Cervenka, K. Watanabe, T. Taniguchi and Y. Chen, *ACS Nano*, 2014, **8**, 1457-1462.
14. M. Yi, Z. Shen, X. Zhao, S. Liang and L. Liu, *Appl. Phys. Lett.*, 2014, **104**, 143101.
15. M. Yi, Z. Shen, W. Zhang, J. Zhu, L. Liu, S. Liang, X. Zhang and S. Ma, *Nanoscale*, 2013, **5**, 10660-10667.
16. L. Liu, Z. Shen, Y. Zheng, M. Yi, X. Zhang and S. Ma, *RSC Adv.*, 2014, **4**, 37726.
17. U. Khan, P. May, A. O'Neill, A. P. Bell, E. Boussac, A. Martin, J. Semple and J. N. Coleman, *Nanoscale*, 2013, **5**, 581-587.
18. U. Khan, A. O'Neill, H. Porwal, P. May, K. Nawaz and J. N. Coleman, *Carbon*, 2012, **50**, 470-475.
19. M. Yi, Z. Shen, X. Zhao, L. Liu, S. Liang and X. Zhang, *Phys. Chem. Chem. Phys.*, 2014, **16**, 11162-11167.
20. M. Yi, W. Zhang, Z. Shen, X. Zhang, X. Zhao, Y. Zheng and S. Ma, *J. Nanopart. Res.*, 2013, **15**, 1811.
21. W. Zhang, M. Yi, Z. Shen, X. Zhao, X. Zhang and S. Ma, *J. Mater. Sci.*, 2012, **48**, 2416-2423.
22. X. Wang, X. Zhao, M. Wang and Z. Shen, *Polym. Eng. Sci.*, 2007, **47**, 1156-1162.
23. M. Wang, X. Zhao, Z. Shen, S. Ma and Y. Xing, *Polym. Degrad. Stabil.*, 2004, **86**, 521-528.
24. K. A. Simonov, N. A. Vinogradov, M. L. Ng, A. S. Vinogradov, N. Mårtensson and A. B. Preobrajenski, *Surf. Sci.*, 2012, **606**, 564-570.
25. M. Petravic, R. Peter, I. Kavre, L. H. Li, Y. Chen, L. J. Fan and Y. W. Yang, *Phys. Chem. Chem. Phys.*, 2010, **12**, 15349-15353.